Cornering Force Maximization with Variable Slip Ratio Control for Independent-All-Wheel-Drive Electric Vehicle

Hiroyuki Fuse, *Student member, IEEE,* and Hiroshi Fujimoto, *Senior member, IEEE*

***Abstract*—The improvement of the maneuverability using fast and precise control of the electric motor is a crucial subject. A driving force controller (DFC) is considered to be a simple yet excellent method to secure the traction of the tire by directly limiting the slip ratio of the wheel. A conventional variable slip ratio limiter (VSRL) used for the DFC changed the limit value according the sideslip angle of the wheel, effectively maximizing either longitudinal or lateral forces of the tire. However, this did not necessarily maximize the cornering force, which is perpendicular to the body speed vector. This study presents a new variable slip ratio control method to maximize the cornering forces when the wheels have a large sideslip angle, with the aim of increasing maximum available lateral acceleration. An improved VSRL is proposed so that even when the sideslip angle of the tire is large, the tire force direction faces perpendicular to the body speed vector and the cornering force can be maximized. Simulations and experimental results using a real EV confirm that cornering maneuverability can be improved, increasing the yaw rate and lateral acceleration during cornering with a large sideslip angle of the tire on slippery roads.**

***Index Terms*—Electric Vehicle, Tire Force Control, Slip Ratio Control, Motion Control, Critical Cornering**

I. Introduction

Electric vehicles (EVs) with individually driven wheels have been extensively studied for advantages concerning motion control. Some of the active subjects are traction control and yaw stability control by torque distribution. Recently, in order to enhance the performance of the traction control, numerous types of controllers have been proposed such as PI(D) control [1], sliding mode control (SMC) [2], fuzzy control [3], and model predictive control (MPC) [4]. As a general trend, most of these studies limit the slip ratio within the optimal slip ratio or certain ranges to prevent the wheels from slipping. In some cases–as seen in [5]–the slip ratio limit is additionally lowered while cornering considering lateral dynamics (such as body sideslip angle and yaw rate).

The yaw stability control and torque distribution law for independent-all-wheel-drive EVs (IAWD-EVs) are also actively studied [2], [6]–[8]. In recent years, concepts of the hierarchical control structure are widely adopted [2], [6]. Typically from top to the bottom, the vehicle dynamics controller mainly determines desired acceleration and yaw rate, the second layer controller determines the torque distribution to each wheel, and the lower controller regulates the slip ratio of each wheel. In [2], four-wheel-independently driven and four-wheel-independently steered EV is considered. The study tried to solve the interference between each independent systems (such as anti-lock braking system, electric stability control, and steering by wire system) by constructing a top-to-bottom integrated motion control. Numerous studies related to the yaw stability control and torque distribution law have achieved various improvements. For example, [7] improves the cornering response analytically by approximately 30% via active torque vectoring control. [8] reduces the handling manipulation effort by 40% using a multiple adaptive sliding mode control. Additionally, for further safety, an advanced driving assistance system (ADAS) is actively studied and applied to commercial passenger vehicles [9]. ADAS concerns variety of controls such as lane keeping assistance, adaptive cruise control, and collision avoidance system.

In order to maximize the effectiveness of the traction control while maintaining the simplicity of the controller, the author's group developed a "driving force controller" (DFC) [10] in 2011 (see Fig. 5). The DFC has a single integrator for the slip ratio control loop with a constant slip ratio limiter (CSRL) and a following PI controller for the wheel speed control. While the CSRL is simple to implement, there are some situations where the lateral force cannot be generated enough owing to the longitudinal slip remaining. In order to increase the lateral force while cornering, a variable slip ratio limiter (VSRL) for the DFC that considers the sideslip angle based on λ-Method tire model was proposed [11]. Basically, when the sideslip angle is large, the VSRL decreases the target slip ratio up to zero. This allows to enhance the cornering performance by effectively generating more lateral forces of tires. However, when the sideslip angle is too large, all the area of the contact patch goes into slippery mode even though the slip ratio (i.e. longitudinal slip) is limited to zero by the VSRL. This could happen when the manually steered vehicle does not have a full active steering system and a driver mistakenly turns the steering wheel excessively. In this case, the lateral force of the tire (especially the front wheels) faces diagonally backward due to the large steering angle. Therefore, the cornering force (perpendicular to the body speed vector) would decrease and undesired deceleration will occur due to the longitudinal component of the lateral force. Since the driver shows an intention of turning by excessively steering, the vehicle should maximize the cornering force.

In order to deal with this problem, this paper proposes an

H. Fuse and H. Fujimoto are with the Department of Advanced Energy, The University of Tokyo, Chiba, 277-8561, Japan e-mail: fuse.hiroyuki17@ae.k.u-tokyo.ac.jp.

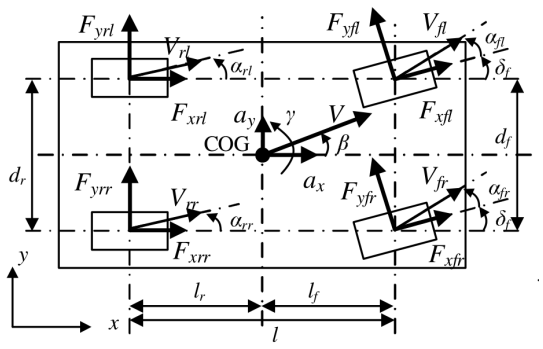

Fig. 1: Vehicle model.

improved version of the VSRL. The main idea is to increase the slip ratio so that the tire force vector faces forward and becomes perpendicular to the body speed vector when sideslip angle is large. This is the discerning point of this study, while most of similar studies are simply trying to decrease the slip ratio.

The effectiveness of the newly proposed VSRL is demonstrated by simulations and experiments using a real EV. The remainder of this paper is as follows. First, the vehicle model and the tire model used for the simulation and the DFC are shown. Second, the detail of the DFC and the conventional VSRL are explained. Third, the newly improved VSRL and its derivation are described. Then, the simulations and experiments and their results are given to confirm its effectiveness.

II. Vehicle model

A. Simplified vehicle model

In this paper, we consider a vehicle model whose wheels are individually driven. Fig. 1 shows an illustration of the vehicle model. In the figure, a_x, a_y, V, β, γ, α, F_x, F_y, and δ_f are longitudinal, lateral acceleration, body speed, body's sideslip angle, yaw rate, sideslip angle, longitudinal force, lateral force of each wheel, and front steering angle, respectively. The subscription of i will be either f or r, indicating front or rear wheel, and j will be either l or r, indicating left or right respectively. For the sake of simplicity, it is assumed that the steering angle of left and right sides is equal. By decomposing the tire force vectors of each wheel and summing up longitudinal, lateral components, we get the equations of motion as follows

$$\begin{aligned} Ma_x &= (F_{xfl}+F_{xfr})\cos\delta_f - (F_{yfl}+F_{yfr})\sin\delta_f \quad (1)\\ &+ (F_{xrl}+F_{xrr}) \\ Ma_y &= (F_{xfl}+F_{xfr})\sin\delta_f + (F_{yfl}+F_{yfr})\cos\delta_f \quad (2)\\ &+ (F_{yrl}+F_{yrr}). \end{aligned}$$

For the rotation motion, we get

$$\begin{aligned} I\dot{\gamma} &= \frac{d_f}{2}(-F_{xfl}+F_{xfr})\cos\delta_f + l_f(F_{xfl}+F_{xfr})\sin\delta_f \\ &+ l_f(F_{yfl}+F_{yfr})\cos\delta_f + \frac{d_f}{2}(F_{yfl}-F_{yfr})\sin\delta_f \\ &+ \frac{d_r}{2}(-F_{xrl}+F_{xrr}) - l_r(F_{yrl}+F_{yrr}), \end{aligned} \quad (3)$$

where I is the yaw moment inertia of the vehicle. Normal reaction force acting on each wheel N_{ij} is obtained by the acceleration of the vehicle. For example, N_{fl} is given by

$$N_{fl} = \frac{l_r}{2l}Mg - \frac{h_g}{2l}Ma_x - \frac{h_g}{2d_f}Ma_y \quad (4)$$

where h_g is the height of the center of the gravity (COG) of the vehicle. This is a quite simple method and a comprehensive yet more reliable method to estimate each load could be seen here [12]. Sideslip angle is geometrically calculated. For example, α_{fl} is given by

$$\alpha_{fl} = \tan^{-1}\frac{V\sin\beta + l_f\gamma}{V - \gamma\frac{d_f}{2}} - \delta_f \approxeq \tan^{-1}V_{fl} - \delta_f. \quad (5)$$

In order to simplify the calculations, we do not consider suspension dynamics (pitch moment and roll moment) or aerodynamics for the simulations.

B. Tire model

A real tire is extremely complicated and various uncertain factors are involved with the generation of the tire force.For analysis or simulations, a lot of tire models have been presented to quantitatively describe the tire force [13] [14] [15], with different focus, degree of complexity, and required parameters.

1) Friction circle: Fig. 2 shows a simplified tire model to consider. In the figure, J_ω, ω, T, r, F, N, θ, and $\mu_{\max}$ are the inertia of the wheel, angular velocity, torque input by traction motors, radius of the tire, resultant force of the tire, normal reaction force acting on the tire, tire force direction, and the maximum friction coefficient, respectively (subscription ij is omitted in the figure). Equation of the rotation of the wheel is given by

$$J_{\omega_i}\dot{\omega_{ij}} = T_{ij} - rF_{xij}. \quad (6)$$

Fundamentally, the torque T causes longitudinal slip due to the difference between the ground speed on the wheel V_{ij} and the rotation speed of the wheel $V_{\omega_{ij}} = r\omega_{ij}$. Combined with the lateral slip, the tire generates its tire force in the same direction of the overall slip. The following equation has to be always satisfied

$$F = \sqrt{F_x^2 + F_y^2} \le \mu_{\max}N. \quad (7)$$

This concept is called a friction circle shown in Fig. 2 (dashed circle). The tire force vector F never goes out of the friction circle. Tire workload η is defined by

$$\eta = \sqrt{F_x^2 + F_y^2}/(\mu_{\max}N) \le 1. \quad (8)$$

Since the maximum available tire force is limited by $\mu_{\max}N$, both longitudinal force F_x and lateral force F_y cannot be maximized simultaneously, which is why the VSRL is important to be able to maximize either of the longitudinal and lateral force effectively.

2) Longitudinal tire model: For the calculation of the tire forces in the simulation, this paper adopts a simplified Magic Formula tire model [14] to represent the longitudinal characteristic (no sideslip angle) as follows.

$$\mu(\lambda) = \mu_{\max} \sin\left(C \tan^{-1} B\left[(1-E)\lambda + \frac{E}{B}\tan^{-1} B\lambda\right]\right) \quad (9)$$

where μ is a friction coefficient, and $\mu_{\max}$ is its maximum value. This simplified Magic Formula can emulate the saturation and the decrease of the friction coefficient when the slip ratio becomes large. λ is a slip ratio which represents the longitudinal slip defined by

$$\lambda_{ij} = (V_{\omega_{ij}} - V_{xij})/\max(V_{\omega_{ij}}, V_{xij}). \quad (10)$$

where V_{xij} is the longitudinal component of V_{ij}. This curve is shown in Fig. 3(a), with parameters of B=11.2757, C=1.3303, E=-0.8501, $\mu_{\max}$ = 0.8. The friction coefficient takes its maximum value $\mu_{\max}$ at a certain slip ratio called optimal slip ratio λ_{p0} when there is no sideslip ($\alpha = 0$). In Fig. 3(a), $\lambda_{\text{p0}} = 0.16$. In the simulation, these parameters are assumed to be constant for simplicity (no change in road surface condition).

3) λ-Method tire model: This study utilizes a tire model called λ-Method to obtain longitudinal force F_x and lateral force F_y from slip ratio λ and sideslip angle α [15]. λ-Method assumes that the tire has a uniform friction characteristic for any direction on the contact patch. Thus, the tire force vector faces towards the same direction of the combined slip occurring. λ-Method only requires a longitudinal tire model which is solely a function of the slip ratio (e.g., λ–μ curve), in order to calculate the tire force vector. λ-Method simply considers both slip and tire force as vectors (extending longitudinal tire model to two-dimensional tire model). Tire force vector $\boldsymbol{f}$ and slip ratio vector $\boldsymbol{\lambda}$ are defined by

$$\boldsymbol{f} = \mu(|\boldsymbol{\lambda}|)N\boldsymbol{\lambda}/|\boldsymbol{\lambda}| \quad (11)$$

$$\boldsymbol{\lambda} = \frac{\boldsymbol{V_w} - \boldsymbol{V}}{\max(|\boldsymbol{V_w}|, |\boldsymbol{V}|)} = \frac{\boldsymbol{V_w} - \boldsymbol{V}}{\max(V_w, V)}, \quad (12)$$

where $\boldsymbol{V_w}$ and $\boldsymbol{V}$ are wheel speed vector parallel to the rotation plane of the wheel, and body speed vector at the point of the wheel, respectively (subscription ij is omitted here).

The norm of the slip ratio vector $|\boldsymbol{\lambda}|$ is represented by slip ratio λ and sideslip angle α. In case of $\lambda > 0$, there are two cases ($|\boldsymbol{V_w}| > |\boldsymbol{V}|$ and $|\boldsymbol{V_w}| < |\boldsymbol{V}|$). The following relations can be obtained geometrically

$$|\boldsymbol{V_w}| > |\boldsymbol{V}| \quad \Leftrightarrow \quad 1 - \lambda > \cos\alpha \quad (13)$$

$$|\boldsymbol{V_w}| < |\boldsymbol{V}| \quad \Leftrightarrow \quad 1 - \lambda < \cos\alpha. \quad (14)$$

In the case of $1 - \lambda > \cos\alpha$, we have

$$|\boldsymbol{\lambda}| = \sqrt{\lambda^2 + (1-\lambda)^2 \tan^2\alpha}. \quad (15)$$

In the case of $1 - \lambda < \cos\alpha$, we have

$$|\boldsymbol{\lambda}| = \sqrt{\sin^2\alpha + \left(\frac{\lambda}{1-\lambda}\right)^2 \cos^2\alpha}. \quad (16)$$

On the other hand, in case of $\lambda < 0$, $|\boldsymbol{V_w}| < |\boldsymbol{V}|$ is always satisfied and the following is geometrically obtained

$$|\boldsymbol{\lambda}| = \sqrt{\sin^2\alpha + \lambda^2 \cos^2\alpha} \quad (17)$$

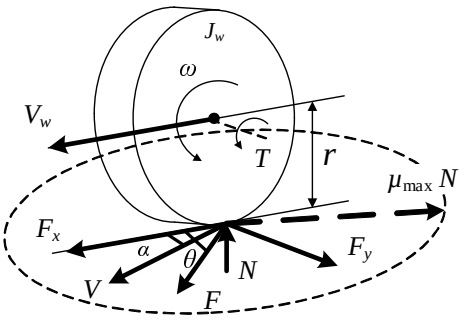

Fig. 2: Tire force and friction circle.

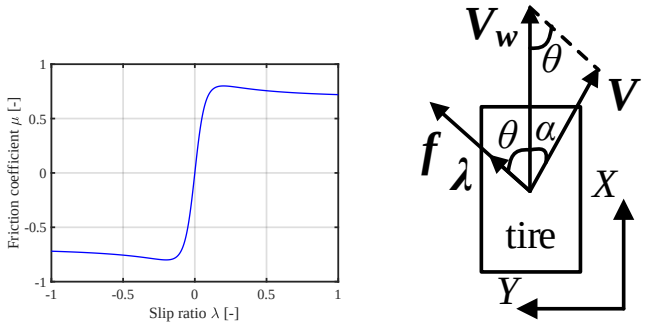

(a) λ–μ curve (longitudinal tire model). (b) λ-Method tire model.

Fig. 3: Tire models.

Fig. 4 shows the tire workload $\eta = \mu/\mu_{\max}$ characteristic graph obtained by λ-Method using the equations above (plotted using the simplified Magic formula tire model with the parameters of B=11.2757, C=1.3303, E=-0.8501, the same with Fig. 3(a).

III. Driving Force Controller

In this section, the previous DFC is explained.

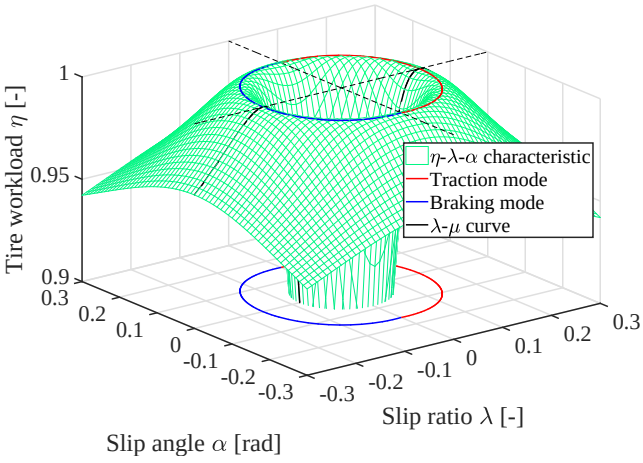

Fig. 4: Tire workload η characteristic. The circle is a set of λ and α where $\eta = 1$ and $|\boldsymbol{\lambda}| = \lambda_{\text{p0}}$ are satisfied. Being outside of the circle means the overall slip becomes too large and available tire force rather decreases, which should be avoided for a stabler and safer maneuver.

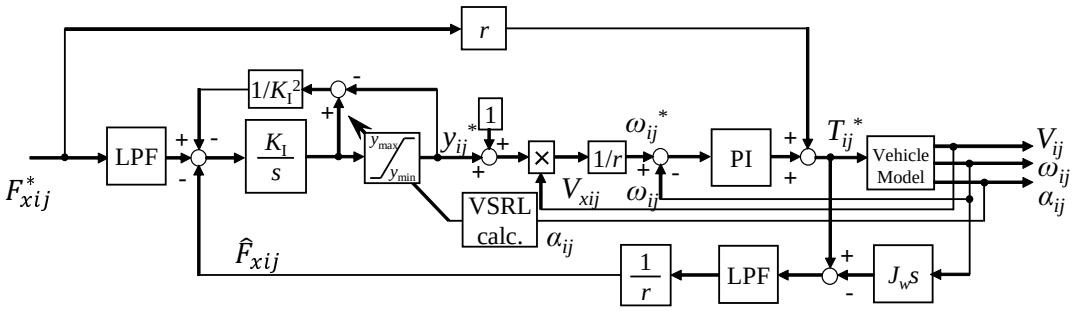

Fig. 5: Driving Force Controller with proposed variable slip ratio limiter.

A. Block diagram and structure

The block diagram of the DFC is shown in Fig. 5. As a demand longitudinal force F_x^* is given by an upper level controller, feedforward loop outputs an approximately adequate torque reference which ignores the inertia of the wheel ($T \approx rF_x$, from (6)). The inner slip ratio and wheel speed control feedback loops adjust the slight error for the precise output.

Generally, the longitudinal force of the tire F_x is nearly proportional to the slip ratio λ in case $\lambda \approx 0$ (Fig. 3(a)), the DFC increases y, which is defined by $y := (V_\omega - V)/V$, using the integrator until desired longitudinal force is achieved. However, since there is a limit to the tire force ($\mu_{\max}$) as explained earlier (see Fig. 3(a) and Fig. 4), we need to add a saturation limit for y, so that the slip ratio can be kept within the range where the friction coefficient μ is a monotonic function of λ. By defining the upper limit $y_{ij\max}$ and the lower limit $y_{ij\min}$ for the integrator, the saturation is applied to the integrator output for limiting y to $y_{ij\min} \leq y_{ij} \leq y_{ij\max}$. With this saturation limit, we can avoid y becoming too large, which prevents the wheel angular speed ω and input torque T becoming too large. In addition, an anti-windup feedback is added to prevent undesired windup phenomena.

B. Previous variable slip ratio limiter

In the previous studies of the DFC, the saturation values of $y_{ij\max}$ and $y_{ij\min}$ are fixed (to be 0.25 and 0.2 respectively, corresponding to $|\lambda| = 0.2$ for example). Considering the friction circle, it is only appropriate in case $\alpha_{ij} = 0$ and there will be a situation that intended lateral force cannot be generated, because the overall slip becomes too large and available tire force rather decreases.

To prevent this problem, Fuse proposed a new method to determine the saturation values of y according to the change of α_{ij} based on λ-Method [11]. λ-Method implies that the norm of the slip ratio vector should be equal or smaller than the optimal slip ratio λ_{p0} in order to effectively maximize available tire force, which is given by

$$|\boldsymbol{\lambda}| \leq \lambda_{\mathrm{p0}}. \tag{18}$$

If sideslip angle α is given,the maximum and minimum slip ratio satisfying the condition are obtained by solving the equations of (15), (16) and (18) for λ as follows

$$\lambda_{\max}(\alpha) = \sin^2\alpha + \cos^2\alpha\sqrt{\lambda_{\mathrm{p0}}^2 - \tan^2\alpha(1-\lambda_{\mathrm{p0}}^2)} \tag{19}$$

$$\lambda_{\min}(\alpha) = \frac{\sqrt{\lambda_{\mathrm{p0}}^2 - \sin^2\alpha}}{\cos\alpha} \tag{20}$$

$\lambda_{\max}$ and $\lambda_{\min}$ are for traction and braking mode, respectively. The loop in Fig. 4 is plotted by the equations above, corresponding to the red line ($\lambda_{\max}$)and blue line ($\lambda_{\min}$) in Fig. 4 The saturation value of y in the DFC is given by

$$y_{\max}(\alpha) = \frac{\sin^2\alpha + \cos^2\alpha\sqrt{\lambda_{\mathrm{p0}}^2 - \tan^2\alpha(1-\lambda_{\mathrm{p0}}^2)}}{\cos^2\alpha + \cos^2\alpha\sqrt{\lambda_{\mathrm{p0}}^2 - \tan^2\alpha(1-\lambda_{\mathrm{p0}}^2)}} \tag{21}$$

$$y_{\min}(\alpha) = \frac{\sqrt{\lambda_{\mathrm{p0}}^2 - \sin^2\alpha}}{\cos\alpha} \tag{22}$$

The previous study successfully demonstrated the increase of the lateral force of the tire and lateral acceleration during cornering [11]. However, if $|\alpha|$ exceeds $\sin^{-1}\lambda_{\mathrm{p0}}$, tire workload η becomes always less than 1 regardless of the slip ratio λ since it is outside of the circle of $\eta = 1$ in Fig. 4 (in that case, the inside of the square root of the above equations of the VSRL becomes negative). Such situations should be avoided by properly adjusting the steering angle if possible. In that case, in order to minimize the slip of the tire, slip ratio reference was set to be $y = 0$ ($|\alpha| > \sin^{-1}\lambda_{\mathrm{p0}}$).

IV. Proposal of a new variable slip ratio limiter

A. Problem with the conventional variable slip ratio limiter

While the previous study was capable of maximizing the tire force,it did not consider the effect of the steering angle δ_f.Therefore, the cornering force, which is perpendicular to the direction of the body speed vector, would not necessarily be maximized and the part of the lateral force of the tire works as a cornering drag force.This is illustrated in Fig. 6.

In the previous VSRL, when $|\alpha_{ij}| > \sin^{-1}\lambda_{\mathrm{p0}}$, the DFC controls the slip ratio λ_{ij} to be zero. Therefore, $V_{wij} = V_{xij}$ holds in Fig. 6(a). Geometrically, the direction of the tire force is diagonally backward by α_{ij} from the direction perpendicular to the body speed vector $\boldsymbol{V_{ij}}$ (a dashed line below). The longitudinal component with respect to the $\boldsymbol{V_{ij}}$ works as cornering drag force, which is $F_{ij}\sin(\alpha_{ij})$.

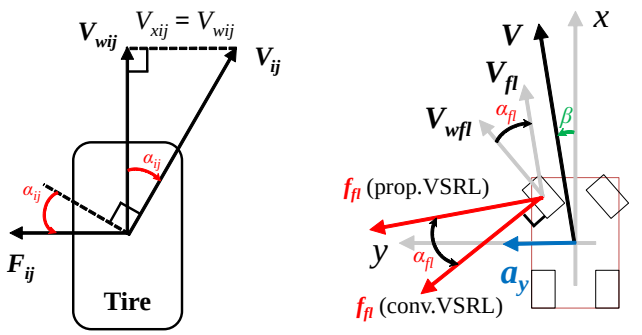

(a) Tire force direction faces diagonally backward by α_{ij}, compared to the direction perpendicular to the body speed vector when $|\alpha_{ij}| > \sin^{-1}\lambda_{\mathrm{p0}}$ with the conventional VSRL.

(b) The proposed VSRL faces the tire force direction perpendicular to the body speed vector by changing the slip ratio limiter, effectively increasing the cornering force.

Fig. 6: Comparison of the tire force direction between the conventional and proposed VSRL when $\alpha_{ij} \geq \sin^{-1}\lambda_{\mathrm{p0}}$.

On the other hand, a newly proposed VSRL changes the slip ratio limiter so that the tire force direction becomes perpendicular to the body speed vector $\boldsymbol{V_{ij}}$ as shown in Fig. 6(b), effectively maximizing the cornering force while decreasing the undesired longitudinal drag force by $F_{ij}\sin(\alpha_{ij})$.

B. Cornering force maximization method

This section derives a desired slip ratio so that the tire force direction becomes perpendicular to the body speed vector and the cornering force can be effectively maximized. Fig. 7 shows an illustration of the proposed method (front left tire is shown here as an example). Here, $\boldsymbol{V_{fl}}$ is the body speed vector at the front left wheel, which is slightly different due to the yaw rotation. In order to direct the tire force $\boldsymbol{f_{fl}}$ perpendicular to the direction of the body speed vector $\boldsymbol{V}$, slip ratio vector $\boldsymbol{\lambda}$ has to be directed in the same direction. Therefore, wheel speed vector $\boldsymbol{V_{wfl}}$ has to be on the dashed line in the left side figure in Fig. 7. Since V-direction component of V_{wfl} and V_{fl} are equal, the following is satisfied

$$V_{fl}\cos(\delta_f - \beta + \alpha_{fl}) = V_{wfl}\cos(\delta_f - \beta). \tag{23}$$

Thus, desired slip ratio $\lambda_{\mathrm{fl-CM}}$ (CM for Cornering force Maximization) is obtained as follows

$$\lambda_{fl-\mathrm{CM}} = 1 - \frac{\cos(\delta_f - \beta)}{\cos(\delta_f - \beta + \alpha_{fl})}\cos\alpha_{fl}. \tag{24}$$

$\lambda_{\mathrm{fl-CM}}$ will be used for the new VSRL in case the sideslip angle is large instead of $\lambda = 0$ (the conventional VSRL).

C. Derivation of limiter-switching sideslip angle

The next thing to do is to obtain the limiter-switching sideslip angle α_{sw} where the VSRL will be switched from the conventional to the new proposed one. When $\alpha = \alpha_{\mathrm{sw}}$, two relations $|\boldsymbol{\lambda}| = \lambda_{\mathrm{p0}}$ (condition of the original VSRL where the tire force becomes maximized) and $\boldsymbol{\lambda} \perp \boldsymbol{V}$ (condition of the cornering force maximization) are satisfied. The limiter-switching sideslip angle α_{sw} can be geometrically obtained from Fig. 7.

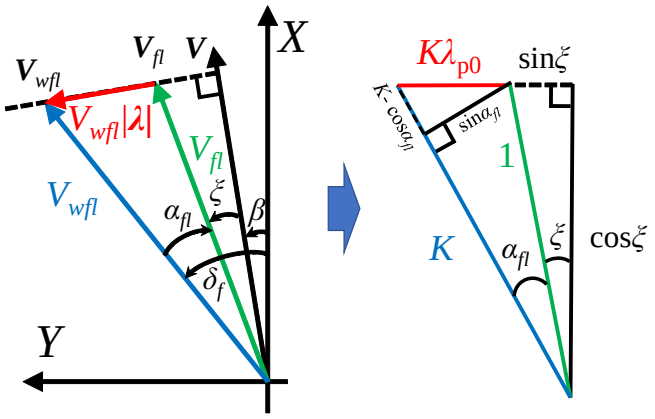

Fig. 7: Illustration of cornering force maximization.

First, since $V_{wfl} > V_{fl}$, slip ratio vector turns out $\boldsymbol{\lambda} = (\boldsymbol{V_{wfl}} - \boldsymbol{V_{fl}})/V_{wfl}$. Therefore, the norm of $\boldsymbol{V_{wfl}} - \boldsymbol{V_{fl}}$ (the length of the red arrow in the left side figure of Fig. 7) is $V_{wfl}|\boldsymbol{\lambda}|$. Since we assume $|\boldsymbol{\lambda}| = \lambda_{\mathrm{p0}}$, we can simplify the geometric relation as shown in the right side figure in Fig. 7. Here, each arrow is divided by V_{fl} and $K = V_{wfl}/V_{fl}$. In this figure, known parameters are ξ and λ_{p0}, while unknown parameters to obtain are K and α_{fl}. From the large right angle triangle, we have this relation

$$K^2 = \cos^2\xi + (K\lambda_{\mathrm{p0}} + \sin\xi)^2. \tag{25}$$

By solving this for K, we get

$$K = \frac{\lambda_{\mathrm{p0}}\sin\xi + \sqrt{1 - \lambda_{\mathrm{p0}}^2\cos^2\xi}}{1 - \lambda_{\mathrm{p0}}^2}. \tag{26}$$

From the small right angle triangle, we have a relation

$$(K\lambda_{\mathrm{p0}})^2 = (K - \cos\alpha_{fl})^2 + \sin\alpha_{fl}^2. \tag{27}$$

By substituting the obtained K and solving the above equation for α_{fl}, we get the limiter-switching sideslip angle α_{sw} represented by

$$\alpha_{\mathrm{sw}} = \cos^{-1}\left(\frac{1 - \lambda_{\mathrm{p0}}^2}{2\left(\lambda_{\mathrm{p0}}\sin\xi + \sqrt{1 - \lambda_{\mathrm{p0}}^2\cos^2\xi}\right)}\right. \tag{28}$$

$$\left. + \frac{\lambda_{\mathrm{p0}}\sin\xi + \sqrt{1 - \lambda_{\mathrm{p0}}^2\cos^2\xi}}{2}\right) \tag{29}$$

$$\xi = \delta_f + \alpha_{fl} - \beta = \tan^{-1}\frac{V\sin\beta + \frac{l_f}{V}\gamma}{V\cos\beta - \frac{d_f}{2}\gamma} - \beta \tag{30}$$

So far, we assume $V_{ij} \neq V$, but usually they are very close to each other and the approximation $V_{ij} \approx V$ does not change α_{sw} much (numerically, four digits are matched to each other in the simulations). In that case, $\xi = 0$ holds and $\lambda_{fl-\mathrm{CM}}$ and α_{sw} are simplified as follows

$$\lambda_{fl-\mathrm{CM}} = \sin^2 \alpha_{fl} \quad (31)$$

$$\alpha_{\mathrm{sw}} = \cos^{-1} \sqrt{1-\lambda_{\mathrm{p0}}^2} = \sin^{-1} \lambda_{\mathrm{p0}} \quad (32)$$

Conveniently, α_{sw} turns out to be no other than $\sin^{-1} \lambda_{\mathrm{p0}}$, exactly the same value where the previous VSRL starts to limit the slip ratio to be zero. Therefore, the newly proposed VSRL limits the slip ratio λ as shown in (21) and (22) when $|\alpha_{ij}| \leq \sin^{-1} \lambda_{\mathrm{p0}}$ just like the conventional VSRL. On the other hand, when $|\alpha_{ij}| > \sin^{-1} \lambda_{\mathrm{p0}}$, the proposed VSRL limits the slip ratio reference values as shown in the following.

$$y_{ij\max}(\alpha) = y_{ij\min}(\alpha) = \tan^2 \alpha_{ij} \quad (|\alpha_{ij}| > \sin^{-1} \lambda_{\mathrm{p0}}) \quad (33)$$

From now on, the newly proposed VSRL ((21), (22), and (33)) is noted as VSRL-CFM (CFM for Cornering Force Maximization).

V. Experimental Verification

An experimental verification of the VSRL-CFM was conducted using an experimental EV.

A. Situation of experiments

The EV approached a slippery road and made a right turn with gradually increasing steering angle (manually done by a driver) while the front wheels were driven by the slip ratio reference at the optimal slip ratio λ_{p0} with the proposed VSRL-CFM. In order to solely evaluate the effect of the VSRL-CFM, the outer feedback loop and the feedforward loop of the DFC were not implemented as shown in Fig. 8.

The setup is emulating a driver presses the accelerator excessively, but tries to make a turn by steering simultaneously. In this situation, the sideslip angle of the front wheels becomes large, precisely emulating the situation where the conventional VSRL has its issue. As the sideslip angle α_{fj} increases, the VSRL-CFM reduces the value of $y_{fj-\max}$. After reaching the limiter-switching sideslip angle $\alpha_{\mathrm{sw}} = \sin^{-1} \lambda_{\mathrm{p0}}$, the VSRL-CFM starts to increase $y_{fj-\max}$ so that the cornering force can be maximized. On the other hand, the rear wheels were driven by a body speed controller to maintain a constant body speed of V_{ref} = 7 m/s (see Fig. 8). By maintaining the constant body speed, cornering maneuverability can be evaluated easily by comparing lateral acceleration a_y, yaw rate γ, and body sideslip angle β. The slip ratio reference and the VSRL-CFM were set with $\lambda_{\mathrm{p0}} = 0.16$, which were obtained in advance [16]. For comparison, the same cornering experiment was tested with the conventional VSRL.

B. Measurement and estimation

The algorithm of the VSRL-CFM controller was coded using Matlab/Simulink. We used a AUTOBOX DS1103 and Control Desk by d-Space to implement the VSRL-CFM controller on the experimental vehicle. With the measurement setup, all the necessary variables (a_x, a_y, γ, V, β, α_{ij}, ω_{ij}, F_{xij}, F_{yij},δ_f, N_{ij}) can be either directly measured or calculated. The lateral force of each wheel F_{yij} cannot be measured by the measurement setup (although it is not required for the VSRL-CFM controller). Although there are studies to estimate F_{yij} [19] using somewhat complex methods, this study only needs those information to estimate the effect of the proposed method. It should be noted that body speed V and body sideslip angle β can be estimated without the use of the optimal velocity sensor as suggested in [17] [18].

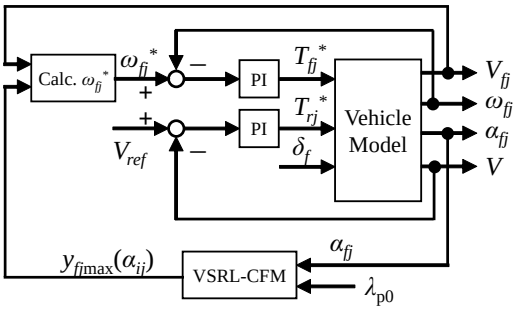

Fig. 8: VSRL-CFM controller and body speed controller for the experimental verification.

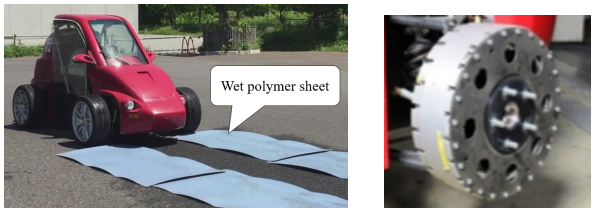

(a) FPEV2–Kanon. (b) In-wheel motor.

Fig. 9: Experimental vehicle and equipped in-wheel motor.

C. Experimental vehicle

In this study, we use a real EV "FPEV2–Kanon" shown in Fig. 9(a) for the experimental verification. The EV is equipped with an direct-drive in-wheel motor (IWM) in each wheel. Tab. I shows the experimental vehicle's specifications.

D. Computer simulation and results

Prior to the experimental verification, the simulations using the vehicle model described in the second chapter were carried out as the confirmation.Tab. II shows the conditions for the simulations. The absolute value of the steering angle was increased from 0 to 0.5 rad by the rate of 0.05 rad/s. The tire model was emulated by Magic formula and λ-Method tire model, with the same parameters shown earlier. The optimal slip ratio of this tire is $\lambda_{\mathrm{p0}} = 0.16$, and maximum friction

TABLE I: Vehicle specification.

Vehicle mass (including driver) M	910 kg
Wheelbase l	1.7 m
Distance from center gravity to front and rear axle l_f,l_r	l_f:1.0 m l_r:0.7 m
Gravity height h_{g}	0.51 m
Front and rear wheel inertia $J_{\omega f}$, $J_{\omega r}$	1.24, 1.26 kg·m^2
Wheel radius r	0.302 m

TABLE II: Conditions of the simulations.

$\lvert\delta_{f\max}\rvert$	$\lvert\dot{\delta_f}\rvert$	λ_{p0}	$\mu_{\max}$	V_{init}
0.5 rad	0.05 rad/s	0.16	0.23	5 m/s

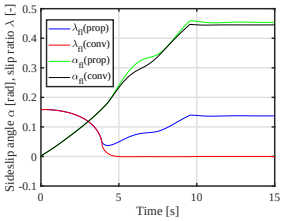

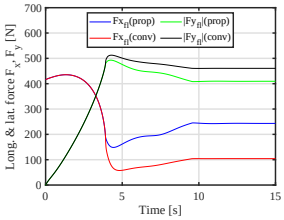

(a) Sideslip angle α and slip ratio λ. (b) Longitudinal and lateral force F_x, F_y.

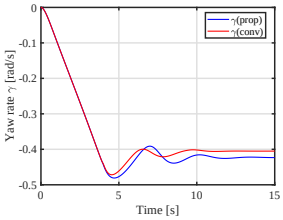

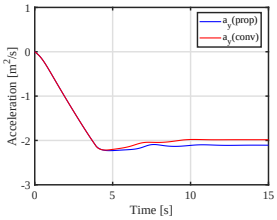

(c) Yaw rate γ. (d) Lateral acceleration A_y.

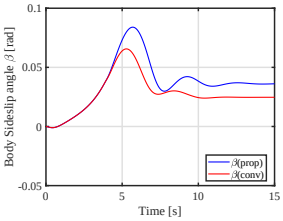

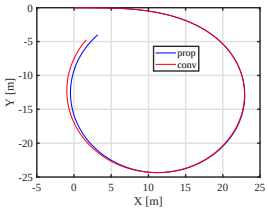

(e) Body sideslip angle β. (f) Vehicle trajectory.

Fig. 10: Simulation results. Compared to the conventional VSRL, the slip ratio of the front wheels λ_{fl} started to increase again when the sideslip angle exceeds $\alpha_{fl} > \sin\alpha_{\mathrm{sw}}$, which is slightly before 5s.

coefficient is $\mu_{\max} = 0.23$. They are close to the conditions of the real experiments.

Fig. 10 shows the simulation results with the conventional VSRL and the proposed VSRL-CFM (only results of front left wheels are shown). As the sideslip angle α_{fl} increases, the slip ratio λ_{fl} inversely decreases during 0 to 4 seconds in the both cases (Fig. 10(a)). Afterwards, it increases again in the case of the VSRL-CFM. With this, the longitudinal and lateral forces F_{xfl}, F_{yfl} change alternatively, as intended (Fig. 10(b)).

The yaw rate γ, lateral acceleration a_y, and body sideslip angle β have larger value while having large sideslip angle (after 10 seconds) compared to the conventional VSRL (Fig. 10(c), Fig. 10(d), Fig. 10(e)). Furthermore, as seen in Fig. 10(f), vehicle turns sharper.

E. Experimental results

The experimental results have generally the same tendency compared to the simulation results (Fig. 11). As the sideslip angle α_{fl} increases up to 0.38 rad, the slip ratio λ_{fl} once decreases but then increases again from around 0.6s in the case of the proposed VSRL-CFM (Fig. 11(a)). The large

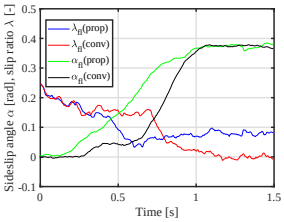

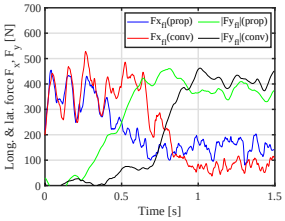

(a) Sideslip angle α and slip ratio λ. (b) Longitudinal and lateral force F_x, F_y.

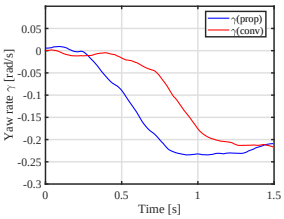

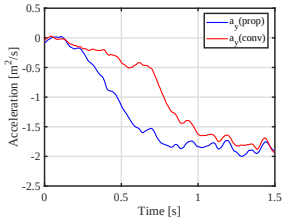

(c) Yaw rate γ. (d) Lateral acceleration A_y.

Fig. 11: Experimental results. The proposed VSRL-CFM has larger maximum yaw rate and lateral acceleration.

increase of the longitudinal force F_{xfl} and the slight decrease of F_{yfl} in case of the proposed VSRL are also the same in the simulations, indicating that the proposed VSRL-CFM worked properly (Fig. 11(b)). The yaw rate γ and lateral acceleration a_y in the case of the VSRL-CFM reach to the larger maximum values by 10% and 5%, respectively.

F. Discussions

According to the simulation results, the proposed new VSRL increases both the yaw rate and lateral acceleration by 5% when the vehicle is turning with the front wheels having a large sideslip angle compared to the previous VSRL. The experimental results basically demonstrate the same tendency with the simulations. Therefore, the proposed VSRL can be useful when a manually steered IAWD-EV is turning with an excessive steering angle mistakenly done by a driver. The proposed VSRL guarantees the maximum lateral acceleration so that the most important request of the driver to turn a curve is fulfilled.

However, by applying the proposed VSRL, the body sideslip angle β also increases so that this control must be enabled only when β is within a certain range (as seen in the envelop controls shown earlier) unless the driver wishes to drive without such assistance (for fun-to-drive). In case the vehicle has a large body sideslip angle β and becomes unstable, longitudinal forces must be generated so that yaw rate can be directly controlled or the vehicle can decelerate (i.e., the VSRL must be deactivated in that case). Further designs of the new VSRL considering the preference of the driver and integration with torque distribution laws and upper vehicle motion controls should be studied. Another thing to discuss is the variation of the optimal slip ratio λ_{p0} because of the change of the road conditions. There are studies to estimate the maximum friction coefficient $\mu_{\max}$ and the optimal slip ratio λ_{p0} seen in [20]. Such the tracking method could be

combined with the proposed VSRL for operating on various conditions of roads.

VI. Conclusion

This study has presented a new variable slip ratio limiter (VSRL) to maximize the cornering force of a manually-steered-independent-all-wheel-drive electric vehicle when the vehicle is turning while the wheels have a large sideslip angle. A new method to determine the VSRL is based on λ-Method tire model so that the tire force face perpendicular to the body speed vector, effectively maximizing the cornering force. The simulation results demonstrated that both yaw rate and lateral acceleration can be increased by 5% when the sideslip angle is quite large during a turn, along with the slight increase of the body sideslip angle and decrease of the turning radius. The experimental results using a real electric vehicle showed the slight increase of the yaw rate, lateral acceleration, and body sideslip angle. These results suggest the plowing of the vehicle can be reduced by the increase of the cornering force.

Acknowledgment

This research was partly supported by Industrial Technology Research Grant Program from New Energy and Industrial Technology Development Organization of Japan (05A48701d), the Ministry of Education, Culture, Sports, Science and Technology grant (22246057 and 26249061).

References

[1] Y. Yang, et al, "Novel Traction Control of Electric Vehicle based on Single Wheel Dynamics," in the Journal of Engineering, vol. 2019, no.23, pp. 9006-9012, 2019.

[2] J. Zhang, W. Sun and H. Du, "Integrated Motion Control Scheme for Four-Wheel-Independent Vehicles Considering Critical Conditions," in IEEE Transactions on Vehicular Technology, vol. 68, no. 8, pp. 7488-7497, Aug. 2019.

[3] D. Yin, N. Sun and J. Hu, "A Wheel Slip Control Approach Integrated With Electronic Stability Control for Decentralized Drive Electric Vehicles," in IEEE Transactions on Industrial Informatics, vol. 15, no. 4, pp. 2244-2252, April 2019.

[4] Y. Ma, J. Zhao, H. Zhao, C. Lu and H. Chen, "MPC-Based Slip Ratio Control for Electric Vehicle Considering Road Roughness," in IEEE Access, vol. 7, pp. 52405-52413, 2019. Slip ratio is strictly limited.

[5] J. Fengjiao, L. Zhiyuan and Z. Hongliang, "A traction control strategy based on optimal slip ratio for the in-wheel motor electric vehicle while steering," 2015 34th Chinese Control Conference (CCC), Hangzhou, 2015, pp. 8171-8176.

[6] Y. Chen, S. Chen, Y. Zhao, Z. Gao and C. Li, "Optimized Handling Stability Control Strategy for a Four In-Wheel Motor Independent-Drive Electric Vehicle," in IEEE Access, vol. 7, pp. 17017-17032, 2019.

[7] L. Zhang, et al, "An Analytical Approach to Improve Vehicle Maneuverability via Torque Vectoring Control: Theoretical Study and Experimental Validation," in IEEE Transactions on Vehicular Technology, vol. 68, no. 5, pp. 4514-4526, 2019.

[8] M. Chae, Y. Hyun, K. Yi and K. Nam, "Dynamic Handling Characteristics Control of an in-Wheel-Motor Driven Electric Vehicle Based on Multiple Sliding Mode Control Approach," in IEEE Access, vol. 7, pp. 132448-132458, 2019.

[9] Haque, Tansu S., et al. "A Review on Driving Control Issues for Smart Electric Vehicles." IEEE Access, 2021.

[10] M. Yoshimura and H. Fujimoto, "Driving torque control method for electric vehicle with in-wheel motors," IEEJ Transactions on Industry Applications, Vol. 131, No. 5, pp.1-8 (2010) (in Japanese).

[11] H. Fuse, H. Fujimoto, "Fundamental Study on Driving Force Control Method for Independent-Four-Wheel-Drive Electric Vehicle Considering Tire Slip Angle," IEEE conference IECON 2018, 2018.

[12] Jeong, Dasol, et al., "Estimation of tire load and vehicle parameters using intelligent tires combined with vehicle dynamics." IEEE Transactions on Instrumentation and Measurement Vol. 70, pp.1-12, 2020.

[13] H. Dugoff, P. Fancher and L. Segel, "Tire Performance Characteristics Affecting Vehicle Response to Steering and Braking Control Inputs," Highway Safety Research Institute of Science and Technology, The University of Michigan, Michigan, technical report, CST 460, Aug 1969.

[14] H. B. Pacejka and E. Bakker, "The Magic Formula Tyre Model," Vehicle System Dynamics: International Journal of Vehicle Mechanics and Mobility, Vol. 21, No. 1, pp. 1-18 (1992).

[15] Y. Horiuchi, "A proposition of the simple tire model for the Vehicle Stability Assist system", Society of Automotive Engineers of Japan, preceding of congress, No.64-98, (1998). (in Japanese)

[16] H. Fuse, et.al., "Minimum-time Maneuver and Friction Coefficient Estimation Using Slip Ratio Control for Autonomously-Driven Electric Vehicle", IEEJ SAMCON2018, 2018.

[17] K. Fujii, H. Fujimoto, "Traction Control based on Slip Ratio Estimation Without Detecting Vehicle Speed for Electric Vehicle", IEEE, Power Conversion Conference, 2007.

[18] C. Geng, et.al.,"Body Slip Angle Estimation and Control for Electric Vehicle with In-Wheel Motors", IEEE conference IECON 2007.

[19] R. A. Cordeiro, et.al., "Estimation of Vertical, Lateral, and Longitudinal Tire Forces in Four-Wheel Vehicles Using a Delayed Interconnected Cascade-Observer Structure," in IEEE/ASME Transactions on Mechatronics, vol. 24, no. 2, pp. 561-571, April 2019.

[20] G. Xu, K. Xu, C. Zheng and T. Zahid, "Optimal Operation Point Detection Based on Force Transmitting Behavior for Wheel Slip Prevention of Electric Vehicles," in IEEE Transactions on Intelligent Transportation Systems, vol. 17, no. 2, pp. 481-490, Feb. 2016.

Hiroyuki Fuse received the B.Eng. degree in Electrical and Electronic Engineering from the Tokyo Institute of Technology in 2017, and the M.S. degree of Advanced Energy from the University of Tokyo in 2019. He is currently pursuing a Ph.D. degree in the Department of Advanced Energy, the University of Tokyo, Japan. He received the JSAE Graduate School Research Award in 2019, IEEJ Excellent Presentation Award in 2019, and the Dean's Award for Outstanding Achievement from the Graduate School of Frontier Sciences and Faculty of Engineering, the University of Tokyo in 2019. His current research interests include vehicle dynamics, and motion control of electric vehicles. He is a student member of IEE of Japan and SAE of Japan, respectively.

Hiroshi Fujimoto received the Ph.D. degree in the Department of Electrical Engineering from the University of Tokyo in 2001. In 2001, he joined the Department of Electrical Engineering, Nagaoka University of Technology as a research associate. From 2002 to 2003, he was a visiting scholar in the School of Mechanical Engineer- ing, Purdue University, U.S.A. In 2004, he joined the Department of Electrical and Computer En- gineering, Yokohama National University, Yoko- hama, Japan, as a lecturer and he became an associate professor in 2005. He is currently an associate professor of the University of Tokyo since 2010. He received the Best Paper Awards from the IEEE Transactions on Industrial Electronics in 2001 and 2013, Isao Takahashi Power Electronics Award in 2010, Best Author Prize of SICE in 2010, the Nagamori Grand Award in 2016, and First Prize Paper Award IEEE Transactions on Power Electonics in 2016. His interests are in control engineering, motion control, nano-scale servo systems, electric vehicle, motor drive, visual servoing, and wireless motors. He is a senior member of IEE of Japan. He is also a member of the Society of Instrument and Control Engineers, the Robotics Society of Japan, and the Society of Automotive Engineers of Japan. He is an associate editor of IEEE/ASME Transactions on Mechatronics from 2010 to 2014, IEEE Industrial Electronics Magazine from 2006, IEE of Japan Transactions on Industrial Application from 2013, and Transactions on SICE from 2013 to 2016. He is a chairperson of JSAE vehicle electrification committee from 2014 and a past chairperson of IEEE/IES Technical Committee on Motion Control from 2012 to 2013.